# PERIODIC RELATIVE ORBITS OF TWO SPACECRAFT SUBJECT TO DIFFERENTIAL GRAVITY AND COULOMB FORCES

Drew R. Jones and Hanspeter Schaub

# 5th International Conference on Spacecraft Formation Flying Missions and Technologies

# PERIODIC RELATIVE ORBITS OF TWO SPACECRAFT SUBJECT TO DIFFERENTIAL GRAVITY AND COULOMB FORCES

**Drew R. Jones**[1] **and Hanspeter Schaub**[2]

[1] *The University of Texas at Austin, WRW Laboratories, 210 E 24th St, Austin, TX 78712, USA*
[2] *University of Colorado, 431 UCB, Boulder, CO 80309, USA*
[1] *drjones604@utexas.edu*
[2] *hanspeter.schaub@colorado.edu*

**Abstract:** *Coulomb forces between charged close flying satellites, can be used for formation control, and constant potentials enable static equilibria. In this work, open-loop time varying potentials, which produce two-craft formation periodic motions are demonstrated for the first time. These are derived in the rotating Hill frame, with linearized gravity, where craft position components are assumed in the form of simple harmonic oscillators. Substitution of the oscillatory functions into the dynamics yields necessary potential histories, to force the periodic orbits. The assumed solutions, however, are not arbitrary, since the dynamical model restricts what oscillatory trajectories are possible. Specifically, a Hill frame integral of motion is derived, and used to show certain candidate periodic functions to be inadmissible. The system dynamics are linearized to analyze stability properties, and it is guaranteed that asymptotic stability is impossible for all solutions. A measure of instability is established via Floquet multipliers of the Monodramy matrix, and this is assessed numerically over free parameter ranges. Lastly, the first order Hill frame model trajectories are repropagated in an inertial frame, with primary disturbances and parameter uncertainty. This illustrates how the orbits may translate to a higher fidelity model, validates Floquet stability claims, and identifies particular solutions that remain near nominal without feedback.*

## 1 Introduction

Spacecraft charge control was considered as early as 1966 by Cover, Knauer, and Maurer [1], who propose using electrostatic forces to inflate and maintain the shape of a large reflecting mesh. Coulomb formations introduced by King et al. [2, 3], refer to the use of this concept in spacecraft formation flying, where the electric potential (or net charge) of each vehicle is actively controlled, to yield desired internal forces. Tightly spaced free-flying craft have many advantages over a single large vehicle, including overall mass reduction, shape changing ability, and multiple launches for deployment, assembly, and repair.[4] Applications for such formations include Earth imaging, surveillance, telescope-occulter pairs, and separated space-borne interferometry.[2] Electric propulsion (EP) systems were initially proposed for controlling the relative motions of formation flying spacecraft. However, EP suffers from limited throttle-ability and introduces the problem of thruster plume impingement, where thruster ejecta may damage or impede neighboring craft.[2] In contrast, active charge control avoids thruster plumes, has fast throttling (millisecond transitions), and can sustain a given force using less power and fuel than EP, yielding specific impulse (ISP) as high as

$10^{13}$ s.[2, 1] Furthermore, active control of spacecraft charge was successfully executed during the SCATHA [5] and ATS [6] missions, and currently on the CLUSTER [7] mission. Other applications for electrostatic thrusting include advanced docking and rendezvous, autonomous inspection, contactless removal of hazardous material[8], and the deployment or retrieval of instruments.[9]

Unfortunately, there are limitations to this electrostatic propulsion system, since the Coulomb forces have limited extent (due to plasma shielding) and are not capable of providing full system controllability.[10] Further challenges arise in accurately modeling the environment dependent Coulomb forces for realistic spacecraft shapes, and in handling the nonlinear dynamical coupling these interactions introduce. Nevertheless, analytical approximate models have been developed and shown to be highly accurate under certain assumptions.[11, 12, 13] One example is the Debye-Hückel equation, that is adopted in the current work, and provides an analytical force law with conservative accounting of plasma shielding.[14]

Coulomb formation equilibria solutions, where constant potentials enable static shapes that appear fixed with respect to their center of mass, are derived and analyzed extensively in the literature.[2, 15, 16, 17, 18, 19, 20] Various researchers, including Berryman and Schaub, state that future investigations should attempt to derive dynamic and periodic Coulomb formation solutions.[9, 21] The first examples of such periodic Coulomb formation solutions are presented here, as well as in Ref. [22]. These serve as natural and desired extensions of the static equilibria. Solutions are defined for two vehicles in the rotating Hill frame, with differential gravity, and where time dependent charge histories provide the necessary forcing to enable the periodic relative orbits. The trajectories are derived by assuming position component solutions; however, the periodic state functions cannot be assumed arbitrarily. Specifically, it is demonstrated that the set of admissible periodic flows is restricted by the underlying dynamics, as well as a Hill frame integral of motion, which is derived in this article. This motion constant, acquired from conservation of the system's inertial angular momentum vector[10], is used to show certain candidate periodic functions are inadmissible.

Various techniques are used to study static Coulomb equilibria stability properties [19, 20, 16], and also in developing continuous feedback controllers to maintain them (often requiring hybrid control).[15, 18, 17, 23, 24] Here the Lyapunov stability of the periodic solutions is analyzed using Floquet theory[25, 26], and asymptotic stability is demonstrated to be impossible, in the linearized sense. Moreover, a measure of instability is assessed numerically using the maximum modulus Floquet multiplier (Monodramy matrix eigenvalue). The state transition matrix associated with these forced periodic solutions, is shown to have many analytical properties in common with those corresponding to periodic orbits, about libration points, in the CRTBP.[27] The stability analyses of periodic Coulomb motions established here, should prove useful in the eventual design of controllers, to maintain and maneuver these open-loop orbits.

Lastly, select solutions are propagated in an inertial frame model that includes nonlinear gravity, primary disturbances, and parameter uncertainties. Such simulations represent the obvious next step in transitioning the ideal solutions to higher fidelity, and this is also done to numerically validate stability claims made using Floquet theory. Moreover, example solutions having maximum modulus Floquet multiplier near

2

unity are demonstrated to remain in the vicinity of nominal when subjected to primary perturbations, all without feedback control. Such solutions are considered invaluable in terms of station-keeping cost.

## 2 Background and Dynamical Model

A conductive craft surface naturally exchanges ions and electrons with the plasma of space, and as a result assumes a non zero electric potential $\phi$, measured in Volts relative to the ambient. The SCATHA satellite[5], launched in 1979, exhibited kV magnitude natural potential at GEO, and therefore modern GEO spacecraft are built to accommodate this, to avoid the negative effects of differential discharge.[4, 2] Furthermore, the naturally occurring potential can be altered artificially, and this technology has been demonstrated on multiple missions.[5, 6, 7] To do so, the charge control device must have sufficient power to supply the desired voltage $\phi$, while continuously emitting particles at a current (rate) at least greater than the incoming environmental current (which tends to drive $\phi$ to natural equilibrium). First order calculations for GEO indicate that starting from $\phi = 0$, a $6$ kV change in spacecraft potential can be achieved in $8$ msec using a mere $200$ mW of power.[2]

### 2.1 Idealized Charging Model

When immersed in a plasma, the ideal vacuum potential of a charged body is limited (or shielded) due to interactions with free particles and photons. This results in a sheath of surrounding (oppositely charged particles) and the Debye length $\lambda_d$ parameterizes the extent of this sheath, and equivalently the strength of the shielding effect. This investigation assumes that $\phi$ is less than the plasma energy, such that the Debye length is dependent only on environmental plasma temperature and density,[28, 12, 11] where experimental data are available. This yields a conservative accounting of the plasma shielding effect, where for nominal conditions $\lambda_d$ is on the order of $0.01$ m at LEO, $200$ m at GEO, and $10$ m at Interplanetary.[12, 11, 29] Throughout this work, a nominal and constant $\lambda_d$ is assumed, and formations near GEO are considered such that $\lambda_d$ is reasonably large (order of $100$ m).[12, 11, 29]
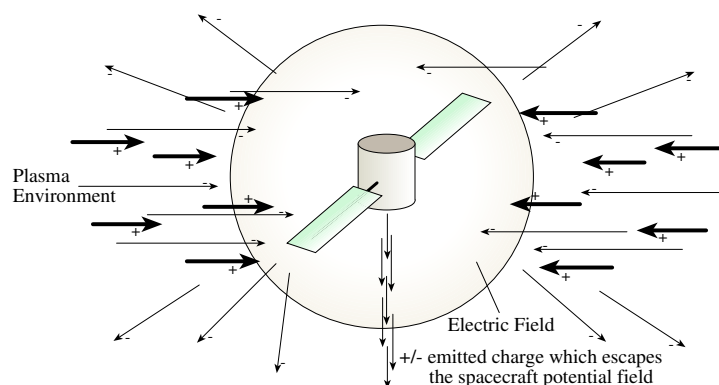


**Figure 1. Outer Sphere Spacecraft Charging in a Plasma Environment [4]**

All spacecraft are idealized here as being spherical, with equal radius $R_{sc}$, and having perfectly conductive outer surface, diagrammed in Fig. 1. This outer shell design (somewhat of an abstraction) provides simplicity, but is also sensible since the potential field of even non spherical craft will approach that of a sphere at sufficiently large radial

distance.[4, 2, 30] Computing the potentials for realistic shapes requires numerical solution of the Vlaslov-Poisson partial differential equations (possibly with finite element analysis techniques), however some of these higher order considerations, including attitude dynamics, are treated in Refs. [4, 2, 28, 12, 31]. Additionally, the capacitance of each spherical craft is assumed to be independent of its neighbors, which is reasonably accurate if the separation distances between vehicles is sufficiently large (relative to $R_{sc}$). The decoupled capacitance approximation is demonstrated numerically to be highly accurate for distances greater than about $10R_{sc}$.[11] Lastly, since formations in the GEO regime are considered, it is reasonable to assume $R_{sc} \ll \lambda_d$, and therefore plasma shielding is neglected over $R_{sc}$. Imposing these assumptions allows for Eq. (1) to analytically relate the net surface charge $q_i$, on craft $i$, to the potential $\phi_i$, where $k_c$ is the Coulomb constant.[28, 11, 15]

$$\phi_i = k_c \frac{q_i}{R_{sc}} \tag{1}$$

Using Eq. (1), the $q_i$ are considered as controls in this research, in substitution for the more likely measurable and controllable parameters $\phi_i$. Moreover, for a 2-craft system, the product of the charges $Q_{12} = q_1 q_2$, is utilized as the control function.

## 2.2 Approximate Electrostatic Model

The electric flux of a closed surface, governed by Gauss's Law, readily shows that the potential field at any point outside the uniformly charged spherical craft, is the same as if the net charge were concentrated at the center of the sphere.[32] Combining this with the well established and frequently adopted Debye-Hückel approximation, leads to the Eq. (2) expression for the potential of a charged spherical craft $i$, at a radial distance $r$ from its center.

$$\phi_i(r) = k_c \frac{q_i}{r} e^{-r/\lambda_d} \tag{2}$$

The Coulomb force exerted by craft $i$ on craft $j$ is then defined as $q_j$ times the gradient of the Eq. (2) potential.[12] This analytical force law is used to provide first order quantitative results for Coulomb formation motions, with a conservative estimate of the plasma shielding effect.[14] The approximate Eq. (1) and Eq. (2) expressions are demonstrated to be highly accurate under nominal GEO conditions, both experimentally and numerically, so long as the Section 2.1 assumptions are maintained.[11, 15] Specifically, that spacecraft capacitances' remain decoupled, $|\phi_i|$ be less than ambient plasma energy, and that $R_{sc} \ll \lambda_d$. Therefore to maintain model accuracy, formations are assumed in a nominal GEO regime, with $r_{ij}$ bounded from below, and with all $|\phi_i|$ of maximum kV order.

## 2.3 Formation Dynamics

With the exception of Sections 6-7, interspacecraft Coulomb forces and the classical gravity force are all that are considered to be acting on the spacecraft. Coulomb force magnitudes considered here are of at least $\mu$N order, and therefore at GEO all perturbing forces are many magnitudes less, and therefore reasonably neglected.[33] An Earth centered inertial frame is denoted $\mathcal{N} : \{\hat{\imath}, \hat{\jmath}, \hat{k}\}$, and $\mathcal{H} : \{\hat{e}_R, \hat{e}_T, \hat{e}_N\}$ denotes the rotating Hill frame, which is centered at and rotates with a nominal center of mass (CM) orbit (assumed circular with radius $R_{cm}$). The axes correspond to $\hat{e}_R$ for radial,

4

$\hat{e}_T$ for transverse (along-track), and $\hat{e}_N$ for normal (orbit-normal). Formation dynamics are considered in the Hill frame as depicted by Fig. 2. Where $\mathbf{R}_i$ and $\mathbf{R}_{cm}$ are position
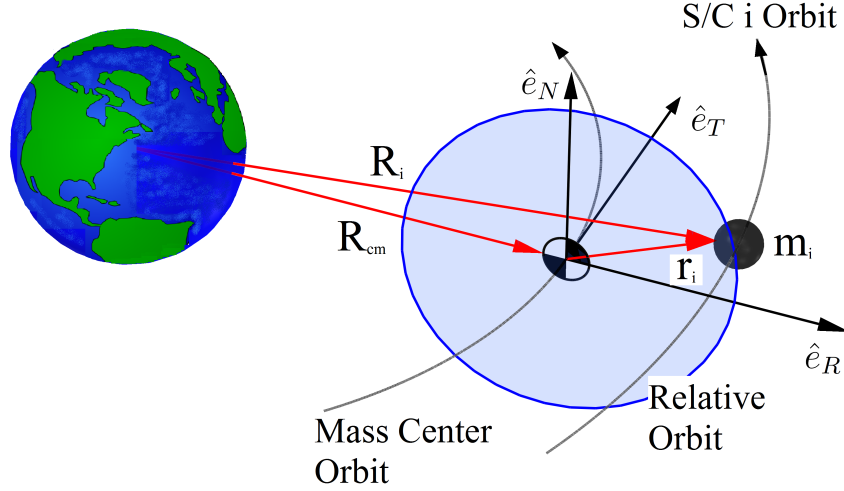


S/C i Orbit

**Figure 2. Relative motion in the rotating hill frame**

vectors of craft $i$ and the formation CM, relative to the $\mathcal{N}$ frame, respectively. And $\mathbf{r}_i$ denotes a craft position vector relative to $\mathbf{R}_{cm}$ (also the origin of the $\mathcal{H}$ frame). Equation (3) relates these position vectors, and the Eq. (4) CM constraint on the $\mathbf{r}_i$ vectors is a consequence of the $\mathcal{H}$ frame definition.

$$\mathbf{R}_i = \mathbf{R}_{cm} + \mathbf{r}_i \tag{3}$$

$$\sum_i m_i \mathbf{r}_i = 0 \qquad \mathbf{r}_i = [x_i \ y_i \ z_i]^T \tag{4}$$

Here $m_i$ is a craft mass, and $x_i$, $y_i$, and $z_i$ are position vector components along the axes $\hat{e}_R$, $\hat{e}_T$, and $\hat{e}_N$.

For an $N$-craft formation, the linearized Clohessy-Wiltshire-Hill equations of relative motion[34] are assumed, along with a net Coulomb acceleration given by the Debye-Hückel approximation.[14] The acceleration of craft $i$, with respect to the rotating Hill frame, is then given by Eq. (5).

$$\ddot{\mathbf{r}}_i = \frac{{}^{\mathcal{H}}\mathrm{d}^2}{\mathrm{d}t^2}\mathbf{r}_i = \begin{bmatrix} 2\omega\dot{y}_i + 3\omega^2 x_i \\ -2\omega\dot{x}_i \\ -\omega^2 z_i \end{bmatrix} + \frac{k_c\,q_i}{m_i}\sum_{\substack{j \\ j \neq i}} \frac{q_j\left(1 + \frac{r_{ij}}{\lambda_d}\right)\mathbf{r}_{ij}}{r_{ij}^3 \exp\left[r_{ij}/\lambda_d\right]} \tag{5}$$

Where $\omega$ denotes the rotational rate of the reference CM orbit (and the $\mathcal{H}$ frame rotational rate), and $r_{ij} = \|\mathbf{r}_i - \mathbf{r}_j\|$ is the separation distance between crafts $i$ and $j$.

## 2.4   Hill Frame Constant of Motion

It is demonstrated here that an $N$-craft Coulomb formation, governed by Eq. (5), admits a scalar constant of motion.[22] Norman and Peck[35] demonstrate that mechanical energy and total angular momentum are conserved, in systems acted on by central body gravity and conservative internal forces. And in general Coulomb forces cannot

alter the system inertial angular momentum vector $\mathbf{H}_0$.[19, 17, 10]

$$\mathbf{H}_0 = \sum_i m_i \left( \mathbf{R}_i \times \frac{{}^{\mathcal{N}}\mathrm{d}}{\mathrm{d}t}\mathbf{R}_i \right) \tag{6}$$

The Eq. (6) $\mathbf{H}_0$ vector can alternatively be written as the sum of two angular momentum terms: $\mathbf{H}_{\mathrm{cm}}$ associated with a total mass $M = \sum_i m_i$ on the CM orbit, and $\mathbf{H}_G$ for the momentum of the individuals moving with respect to the CM. It is important to note that no dynamical simplifications have been made, thus far.

$$\mathbf{H}_0 = M \left( \mathbf{R}_{\mathrm{cm}} \times \frac{{}^{\mathcal{N}}\mathrm{d}}{\mathrm{d}t}\mathbf{R}_{\mathrm{cm}} \right) + \sum_i m_i \left( \mathbf{r}_i \times \frac{{}^{\mathcal{N}}\mathrm{d}}{\mathrm{d}t}\mathbf{r}_i \right) \tag{7a}$$

$$\mathbf{H}_0 = \mathbf{H}_{\mathrm{cm}} + \mathbf{H}_G \tag{7b}$$

Inherent to the Hill frame definition is the assumption that $\mathbf{H}_{\mathrm{cm}}$ is constant. With this assumption, Eqs. (7a)-(7b) imply that $\mathbf{H}_G$ is constant. Also, the reference orbit plane $\hat{e}_R$-$\hat{e}_T$ is assumed coplanar to the $\hat{\imath}$-$\hat{\jmath}$ plane (an arbitrary choice). Therefore, $\mathcal{H}$ is obtained by rotating $\mathcal{N}$, about $\hat{k} = \hat{e}_N$, at the constant rate $\omega$ (also inherent to the Hill frame definition). The angular velocity vector of the $\mathcal{H}$ frame is then $\boldsymbol{\omega} = \omega\hat{k} = \omega\hat{e}_N$. The vector $\mathbf{H}_G$ transformed to the rotating Hill frame, is denoted $\mathbf{h}_G$, and its time derivative with respect to the $\mathcal{H}$ frame, is computed by the transport theorem.

$$\frac{{}^{\mathcal{H}}\mathrm{d}}{\mathrm{d}t}\mathbf{h}_G = \frac{{}^{\mathcal{N}}\mathrm{d}}{\mathrm{d}t}\mathbf{H}_G - (\boldsymbol{\omega} \times \mathbf{h}_G) = \begin{bmatrix} 0 \\ 0 \\ 0 \end{bmatrix} - \begin{bmatrix} -\omega h_y \\ \omega h_x \\ 0 \end{bmatrix} \tag{8a}$$

$$^{\mathcal{H}}\mathbf{h}_G = [\, h_x \ h_y \ h_z \,]^T \tag{8b}$$

Where $\mathbf{h}_G$ is defined component wise (in the $\mathcal{H}$ basis) by Eq. (8b). Since $\mathbf{H}_G$ is a constant vector, Eqs. (8a)-(8b) indicate $h_z$ to be a scalar constant of motion for Hill frame formations involving internal forces (e.g. Coulomb forces). This result is summarized in Eqs. (9a)-(9b), with $h_z$ written in terms of spacecraft coordinates, and its time derivative taken with respect to the $\mathcal{H}$ frame.

$$h_z = \sum_i m_i \left( x_i \dot{y}_i - y_i \dot{x}_i \right) \tag{9a}$$

$$\dot{h}_z = \frac{{}^{\mathcal{H}}\mathrm{d}}{\mathrm{d}t}h_z = \sum_i m_i \left( x_i \ddot{y}_i - y_i \ddot{x}_i \right) = 0 \tag{9b}$$

Where position vector time derivatives $\dot{\mathbf{r}}_i$, taken with respect to the $\mathcal{H}$ frame, are related to inertial time derivatives, via the transport theorem.

$$\dot{\mathbf{r}}_i = \frac{{}^{\mathcal{H}}\mathrm{d}}{\mathrm{d}t}\mathbf{r}_i = \frac{{}^{\mathcal{N}}\mathrm{d}}{\mathrm{d}t}\mathbf{r}_i - (\boldsymbol{\omega} \times \mathbf{r}_i) = \begin{bmatrix} \dot{x}_i \\ \dot{y}_i \\ \dot{z}_i \end{bmatrix} \tag{10}$$

Interestingly, conservation of only the out-of-plane component of angular momentum is a well known result in the case of spacecraft formations in a spherical gravity model, with the inclusion of $J_2$.[36] However, in that problem it is an inertial angular momentum quantity, as opposed to the Hill frame quantity derived here.

6

## 2.5  Reduced and Normalized Two-Craft Dynamics

The following reduced and scaled equations of motion govern the 2-craft system, and simplify subsequent analyses. A scaled charge product $\tilde{Q}_{12}$, given by Eq. (11), is substituted into the Eq. (5) expression. The scaling introduces a time transformation into the equations of motion, to the non dimensional time-like variable $\tau$. This transform is defined by Eq. (12), for a dummy variable $\zeta$.

$$\tilde{Q}_{12} = \frac{k_c\,Q_{12}}{\omega^2} \tag{11}$$

$$\mathrm{d}\tau = \omega\mathrm{d}t \qquad (\zeta)' = \frac{\mathrm{d}\zeta}{\mathrm{d}\tau} = \frac{1}{\omega}\frac{\mathrm{d}\zeta}{\mathrm{d}t} \tag{12}$$

The Eq. (4) CM constraint is then used to explicitly remove $\mathbf{r}_2$ terms from the resulting craft 1 acceleration. This yields reduced and normalized equations of motion for the system, with $\Psi$ and $M_{r1}$ used as auxiliary terms, and the craft 1 subscript omitted for simplicity (i.e. $\mathbf{r} = \mathbf{r}_1$).

$$\mathbf{r}'' = \frac{\ddot{\mathbf{r}}}{\omega^2} = \begin{bmatrix} 2y' + 3x \\ -2x' \\ -z \end{bmatrix} + \tilde{Q}_{12}\,\Psi(r) \begin{bmatrix} x \\ y \\ z \end{bmatrix} \tag{13a}$$

$$\Psi(r) = \frac{M_{r1}^2\left(1 + \frac{r}{M_{r1}\lambda_d}\right)}{m_1\,r^3\,\exp\left[\frac{r}{M_{r1}\lambda_d}\right]} \qquad M_{r1} = \frac{m_2}{m_1 + m_2} \tag{13b}$$

Equations (13a)-(13b) therefore define the craft 1 acceleration (in the variable $\tau$), as a function of its own position vector $\mathbf{r}_1$, its own scaled velocity vector $\mathbf{v}_1 = \mathbf{r}_1' = \dot{\mathbf{r}}_1/\omega$, and $\tilde{Q}_{12}$. These dynamics are utilized throughout; however, it is often informative to consider the dimensional craft 1 potential $\phi_1$ (in Volts), rather than $\tilde{Q}_{12}$. Therefore, transformations from $\tilde{Q}_{12}$ to the net charge $q_1$ (and potential $\phi_1$) are defined in Eq. (14).

$$q_1 = \omega\sqrt{\frac{|\tilde{Q}_{12}|}{k_c}} \qquad \phi_1 = \frac{\omega\sqrt{k_c|\tilde{Q}_{12}|}}{R_{sc}} \tag{14}$$

Where positive $q_1$, and equal charge magnitude ($|q_1| = |q_2|$) conventions are adopted, and Eq. (1) relates $q_1$ to $\phi_1$.

The Hill frame motion constant $h_z$ may also be rewritten for the special case of two vehicles, in the non dimensional variable $\tau$. To do this, Eq. (4) is used to explicitly eliminate craft $2$ state variables from Eqs. (9a)-(9b), and then the Eq. (12) transform is applied. This yields the Eq. (15) 2-craft integral of motion, and its $\mathcal{H}$ frame derivative is given by Eq. (16).

$$h_z = \frac{\omega\left(m_1^2 + m_1 m_2\right)}{m_2}\left[x(\tau)y'(\tau) - y(\tau)x'(\tau)\right] \tag{15}$$

$$h_z' = x(\tau)y''(\tau) - y(\tau)x''(\tau) = 0 \tag{16}$$

## 3 Analytical Stability of Periodic Solutions

Equations (13a)-(13b) may be written in the 1st order ODE system form of Eq. (17), where $\tau$ is the independent variable of integration, $\mathbf{X}(\tau)$ denotes a state vector, and $\mathbf{F} = \mathbf{X}'(\tau)$ its derivative taken with respect to the rotating Hill frame.

$$\mathbf{X}' = \mathbf{F}\left(\mathbf{X},\ \tilde{Q}_{12},\ \tau\right) \tag{17}$$

Closed solution curves that satisfy Eq. (17), are denoted by a reference state trajectory $\mathbf{X}^*(\tau)$, and a reference feed-forward control $\tilde{Q}(\tau) = \tilde{Q}_{12}^*(\tau)$. A zero-input linearization of Eq. (17) about a periodic reference solution, with non dimensional time period $\tau_p$ (dimensional $t_p$), yields the Eq. (18) linear ODE system.

$$\delta\mathbf{X}'(\tau) = \left(\frac{\partial\mathbf{F}}{\partial\mathbf{X}}\right)\bigg|_{\left(\mathbf{X}^*,\tilde{Q}\right)} \delta\mathbf{X}(\tau) = \mathbf{A}(\tau)\,\delta\mathbf{X}(\tau) \tag{18}$$

This governs the dynamics of small state perturbations $\delta\mathbf{X}(\tau)$ about $\mathbf{X}^*(\tau)$, and the non-autonomous state propagation matrix $\mathbf{A}(\tau)$ is also $\tau_p$ periodic.[37, 26] Moreover, there exists a state transition matrix $\mathbf{\Phi}(\tau,0)$, that maps $\delta\mathbf{X}$ from $0 \to \tau$ (initial $\tau$ assumed zero), in accordance with Eq. (19).

$$\delta\mathbf{X}(\tau) = \mathbf{\Phi}(\tau,0)\,\delta\mathbf{X}(0) \qquad \mathbf{\Phi}'(\tau,0) = \mathbf{A}(\tau)\,\mathbf{\Phi}(\tau,0) \tag{19}$$

The state propagation matrix $\mathbf{A}(\tau)$ specific to Eqs. (13a)-(13b) is derived in Eqs. (20a)-(20b), where $\mathbf{0}$ and $\mathbf{I}$ denote $3x3$ zero and identity matrices, respectively.

$$\mathbf{A}(\tau) = \left[\begin{array}{c|c} \mathbf{0} & \mathbf{I} \\ \hline \frac{\partial\mathbf{r}''}{\partial\mathbf{r}} & \frac{\partial\mathbf{r}''}{\partial\mathbf{v}} \end{array}\right]\bigg|_{\left(\mathbf{X}^*,\tilde{Q}\right)} = \left[\begin{array}{c|c} \mathbf{0} & \mathbf{I} \\ \hline \mathbf{G} & \mathbf{H} \end{array}\right] \qquad \mathbf{H} = \begin{bmatrix} 0 & 2 & 0 \\ -2 & 0 & 0 \\ 0 & 0 & 0 \end{bmatrix} \tag{20a}$$

$$\mathbf{G}(\tau) = \begin{bmatrix} 3 & 0 & 0 \\ 0 & 0 & 0 \\ 0 & 0 & -1 \end{bmatrix} + \tilde{Q}(\tau)\,\Psi(r)\left[\left(\mathbf{I} - \frac{3\mathbf{r}\mathbf{r}^T}{r^2}\right) - \frac{\mathbf{r}\mathbf{r}^T}{M_{r1}\lambda_d\left(r + M_{r1}\lambda_d\right)}\right] \tag{20b}$$

Where $\Psi(r)$ is defined in Eq. (13b), and $\mathbf{r} = \mathbf{r}_1^*$ denotes a craft 1 reference ($\tau$ dependent) position vector. The $\mathbf{A}(\tau)$ matrix has the same form as the linearized dynamics about libration points in the CRTBP.[27] And consequently, $\mathbf{\Phi}$ is similarly symplectic according to Eq. (21), for the constant skew-symmetric matrix $\mathbf{J}$.

$$\mathbf{J}\mathbf{A}^T = -\mathbf{A}\mathbf{J} \qquad \mathbf{\Phi}\mathbf{J}\mathbf{\Phi}^T = \mathbf{J} \qquad \mathbf{J} = \left[\begin{array}{c|c} \mathbf{0} & \mathbf{I} \\ \hline -\mathbf{I} & \mathbf{H} \end{array}\right] \tag{21}$$

The matrix $\mathbf{\Phi}(\tau_p,0)$ is known as the Monodramy matrix. Floquet multipliers $\sigma$, correspond to the Monodramy matrix eigenvalues, and may be used to access zero-input Lyapunov stability of $\mathbf{X}^*(\tau)$. Specifically, the orbit is unstable if any $|\sigma_i| > 1$ (and/or if any repeated $|\sigma_i| = 1$ is not semisimple).[25, 26] Also, since $\mathbf{\Phi}(\tau_p,0)$ satisfies Eq.(21), it exhibits the following properties[26]

    1. $\det(\mathbf{\Phi}) = |\mathbf{\Phi}| = 1$

2. At least one Floquet multiplier has modulus of unity: $|\sigma_i| = 1$

3. The $\sigma_i$ appear in reciprocal pairs (i.e. if $\sigma_i$ is eigenvalue, then so is $\sigma_j = 1/\sigma_i$)

These are the same properties as associated with periodic orbits about libration points in the CRTBP[27], and the latter property entails that a stable $\sigma_i$ (inside the unit circle) has a corresponding unstable $\sigma_j$ (outside the unit circle). The maximum modulus Floquet multiplier, denoted $|\sigma|_{\mathsf{max}}$, is used in this research as a measure of relative instability, between particular $\mathbf{X}^*(\tau)$ solutions. Based on Floquet theory[25], stability categories for periodic solutions to Eq. (18), are summarized in Table 1. These

**Table 1.  Floquet Stability of Periodic Coulomb Formations**

| Category | Lyapunov Stability |
|---|---|
| $|\sigma|_{\mathsf{max}} = 1$ | |
|   All repeated $|\sigma_i| = 1$ are semi-simple | Uniform Stable |
|   Any repeated $|\sigma_i| = 1$ is not semi-simple | Unstable |
| $|\sigma|_{\mathsf{max}} > 1$ | Unstable |

categories imply that asymptotic stability is impossible for all 2-craft periodic Coulomb formations, and at best such solutions will exhibit linearized uniform stability (boundedness). Furthermore, $\mathbf{X}^*(\tau)$ will have identical stability in the Eq. (17) nonlinear system, if the linearized system exhibits significant behavior (i.e. $|\sigma|_{\mathsf{max}} > 1$).[26]

## 4  Periodic Coulomb Formations via Assumed Solutions

The reference spacecraft position components ($x$, $y$, and $z$) are assumed to take the form of simple harmonic oscillators. The presented analyses are specific to these solutions, which happen to conserve total mechanical energy. Other periodic motions, having assumed functions described by different finite Fourier series, may exist, but are outside the scope of this work. However, the assumed periodic functions are not arbitrary, because the set of allowed motions is restricted, and some example candidate functions are shown in Section 4.3 to be inadmissible. The Coulomb forces are not conservative by definition, but the open-loop potential functions considered here are explicitly dependent on spacecraft coordinates, and therefore nonconservative Coulomb forcing is also outside of the current scope.

Furthermore, coupling in Eqs. (13a)-(13b), insist that a periodic solution has both $x$ and $y$ components, otherwise it has only a $z$ component. Therefore, three possible periodic orbit types are permitted: $\hat{e}_N$ axis only (out-of-plane), $\hat{e}_R$-$\hat{e}_T$ planar motions (in-plane), and full state motions. Attention here is limited to the latter two orbit families, but those solutions which oscillate along only the $\hat{e}_N$ axis are covered in Ref. [22].

### 4.1  In-Plane Periodic Motions

These dynamic solutions are derived using only the $\hat{e}_R$-$\hat{e}_T$ components of Eqs. (13a)-(13b), since the $\hat{e}_N$ component decouples to 1st order. It is assumed that $x(\tau)$ and $y(\tau)$ are simple harmonic oscillators (both with period $\tau_p$), defined by Eq. (22), where

$A_x$ and $A_y$ denote amplitudes of oscillation.

$$x(\tau) = A_x \cos(\theta\tau) \qquad y(\tau) = A_y \sin(\theta\tau) \qquad (22)$$

Therefore, oscillations occur about $x = y = 0$, with the initial condition $x(0) = A_x$, $y(0) = 0$. The oscillation frequency $\theta$ is related to the relative orbit period $t_p$ (and non dimensional period $\tau_p$) via Eq. (23).

$$\theta = \left(\frac{2\pi}{\tau_p}\right) = \left(\frac{2\pi}{\omega\, t_p}\right) \qquad (23)$$

The Eq. (22) terms and their time derivatives are then substituted into Eq. (13a), and the resulting $\hat{e}_R$ and $\hat{e}_T$ acceleration terms are divided by $x(\tau)$ and $y(\tau)$, respectively. Rearranging such that the Coulomb acceleration terms are on the left hand side, results in Eqs. (24a)-(24b), with $\Psi(r)$ as defined in Eq. (13b).

$$\tilde{Q}_{12}(\tau)\,\Psi(r) = -\theta^2 - 3 - 2\theta\left(\frac{A_y}{A_x}\right) \qquad (24a)$$

$$\tilde{Q}_{12}(\tau)\,\Psi(r) = -\theta^2 - 2\theta\left(\frac{A_x}{A_y}\right) \qquad (24b)$$

Equating the right hand side of Eq. (24a) and Eq. (24b) leads to the quadratic equation.

$$\left(\frac{A_y}{A_x}\right) = \frac{-3 \pm \sqrt{9 + 16\theta^2}}{4\theta} \qquad (25)$$

There are two real solutions to Eq. (25) for all $\tau_p > 0$, since $\sqrt{9 + 16\theta^2}$ is always real. This constraint on the assumed motion insists that $A_x \neq A_y$, meaning that the resulting relative orbit is an ellipse about the CM. By choosing the initial condition $A_x > 0$, two cases, corresponding to the two roots of the quadratic, may be defined.

- *Case A (+ root):* Ellipse major axis is $A_x$, and minor axis is $A_y$ ($A_x > A_y$).

- *Case B (− root):* Ellipse major axis is $-A_y$, and minor axis is $A_x$ ($A_x < |A_y|$).

The necessary feed-forward charge history is derived from either Eq. (24a) or Eq. (24b), with the substitution of Eq. (25). This yields $\tilde{Q}(\tau)$ as an explicit function of $x(\tau)$ and $y(\tau)$, since $r^2(\tau) = x^2(\tau) + y^2(\tau)$.

$$\tilde{Q}_{12}(r(\tau)) = \frac{-1}{\Psi(r)}\left[\theta^2 + 3 + \left(\frac{-3 \pm \sqrt{9 + 16\theta^2}}{2}\right)\right] \qquad (26)$$

The Eq. (26) function provides the forcing for the assumed trajectory, and is itself a simple oscillator. However, its oscillations are offset from zero, and with period of $\tau_p/2$. Additionally, when $\tau_p = 2\pi$, $t_p$ is equal to the CM orbital period ($\approx$ 1 day), and the relative orbit has major axis twice that of minor axis. The entire family of these periodic relative orbits, in the $\hat{e}_R$-$\hat{e}_T$ plane, are generated as follows.

1. Choose $A_x$, and either Case A or Case B of Eq. (25)

2. Solve $A_y$ via Eq. (25)

3. Propagate the open-loop system with $\tilde{Q}(\tau)$ defined by Eq. (26)

## 4.2 Full State Periodic Motions

If $x$, $y$, and $z$ are all assumed to be, $\tau_p$ periodic, simple oscillators the only solution is a trivial non Coulomb solution: $\tilde{Q}(\tau) = 0$, $\theta = 1$, and $A_y/A_x = -2$. However, if $x(\tau)$ and $y(\tau)$ are defined as in Eq. (22), and $z(\tau)$ is defined as in Eq. (27), non trivial full state periodic motions are admitted.

$$z(\tau) = A_z \sin\left(B_z \theta \tau\right) \qquad B_z = \ldots \frac{1}{8}, \frac{1}{4}, \frac{1}{2}, 2, 4, 8 \ldots \tag{27}$$

For fractional $B_z$, the relative orbits are $\tau_p/B_z$ periodic (with $1/B_z$ planar oscillations in a full cycle). Whereas for integer $B_z$, the relative orbits are $\tau_p$ periodic (with $B_z$ orbit-normal oscillations in a cycle). Substituting the assumed solutions (and their derivatives), along with Eq. (25) into Eqs. (13a)-(13b), and rearranging, leads to Eq. (28).

$$\tilde{Q}(\tau)\Psi(r) = \left(1 - B_z^2 \theta^2\right) = -\theta^2 - 2\theta \left(\frac{4\theta}{-3 \pm \sqrt{9 + 16\theta^2}}\right) \tag{28}$$

It is inferred from this expression that $\tau_p$ is no longer free, but rather is dependent on $B_z$. Furthermore, Eq. (28) can be rewritten in the form of Eq. (29), a nonlinear root-finding function, in the variable $\theta$. For integer $B_z$ values, there exists a unique real-valued $\theta$ which satisfies Eq. (29), for both roots of the Eq. (25) quadratic. In contrast, fractional $B_z$ values admit no real-valued $\theta$ solutions, for either root of the quadratic.

$$8\theta^2 + \left(-3 \pm \sqrt{9 + 16\theta^2}\right)\left[\theta^2(1 - B_z^2) + 1\right] = 0 \tag{29}$$

This numerical result means that the least period of $z(\tau)$ oscillations must be strictly less than the in-plane least period. Solutions are thereby limited to the subset of even integer $B_z$, such that $\hat{e}_N$ axis oscillations occur $B_z$ times during $\tau_p$. The amplitudes $A_x$ and $A_z$ are free, and so is $B_z$ (in the subset of even integers). This leads to multiple families of three dimensional (in position), dynamic and periodic orbits. Orbits within the families are generated as follows.

1. Choose $A_x$, $A_z$, and $B_z$ (even integer)

2. Choose either Case A or Case B of Eq. (25)

3. Solve $\theta$ (and $\tau_p$) numerically from Eq. (29)

4. With $\theta$ known, solve $A_y$ via Eq. (25)

5. Propagate the open-loop system with $\tilde{Q}(\tau)$ defined by Eq. (26)

## 4.3 Restrictions on Assumed Periodic Trajectories

The Eq. (16) constant of motion insists that $x(\tau)$ and $y(\tau)$ periodic functions are not assumed arbitrarily. The following are demonstrable examples of simple periodic functions, which cannot satisfy this constraint, and therefore such motions cannot occur.

- *General simple harmonic oscillation, about the origin:*

$$x(\tau) = A_x \cos{(\theta_x \tau)} \qquad y(\tau) = A_y \sin{(\theta_y \tau)} \qquad (30)$$

Substituting these into Eq. (16) yields $\theta_y^2 = \theta_x^2$, and since $\theta > 0$ it is concluded that $\theta_x = \theta_y$. Therefore, Eq. (30) periodic flows having $\theta_x \neq \theta_y$ cannot exist. Hence $\theta_x = \theta_y = \theta$ is explicitly assumed in Eq. (22).

- *General rotary motion (periodic polar curve):*

$$r(\tau) = A_x + A_y \sin{(n\theta\tau)} \qquad (31a)$$
$$x(\tau) = r(\tau) \ \cos{(n\theta\tau)} \qquad (31b)$$
$$y(\tau) = r(\tau) \ \sin{(n\theta\tau)} \qquad (31c)$$

Where $n$ is a positive integer and $A_y \neq 0$. Evaluating the Eq. (16) condition for the assumed solution of Eqs. (31a)-(31c), yields the following expression.

$$2nA_y \cos{(n\theta\tau)} \left[ A_y \sin{(n\theta\tau)} + A_x \right] = 0 \qquad (32)$$

Equation (32) is invalid for some $\tau$, and therefore by contradiction this motion is not admitted.

- *General simple harmonic oscillation, offset from the origin:*

$$x(\tau) = x_0 + A_x \cos{(\theta_x \tau)} \qquad (33a)$$
$$y(\tau) = y_0 + A_y \sin{(\theta_y \tau)} \qquad (33b)$$

If either $x_0$ or $y_0$ are zero, then Eq. (16) and Eqs. (33a)-(33b) insist either $x(\tau)$ or $y(\tau)$ are constant. This is a contradiction. The Eq. (16) momenta condition is satisfied, however, for $x_0 \neq 0$, $y_0 \neq 0$, and $\theta_x = \theta_y$. But it is readily shown from the governing dynamics, that no real-valued $\tilde{Q}(\tau)$ history can enable that motion. This example demonstrates that Eq. (16) is a necessary (but not sufficient) condition for Coulomb formation periodic orbits, since an assumed trajectory can satisfy Eq. (16), but not represent a real solution to Eqs. (13a)-(13b).

## 5  Numerically Simulated Periodic Coulomb Formations

The following results are generated by propagating the dynamical system in Eqs. (13a)-(13b) numerically, using the Table 2 constant values. Where equal mass and radius vehicles are assumed, and a mean value for $\lambda_d$ at GEO is adopted. [29]

### Table 2.  Numerical Simulation Constant Parameters

| Parameter | Value | Units |
|-----------|-------|-------|
| $R_{\text{cm}}$ | $4.227e^7$ | m |
| $R_{sc}$ | 1 | m |
| $\lambda_d$ | 180 | m |
| $m_i$ | 150 | kg |
| $\omega$ | $7.2593e^{-5}$ | rad/s |
| $k_c$ | $8.99e^9$ | Nm$^2$ / C$^2$ |

## 5.1 In-Plane Periodic Motions

Example craft 1 position histories for $A_x = 20$ m and $\tau_p = \pi$ are presented in Fig. 3(a)-3(b), along with corresponding potential histories in Fig. 4(a)-4(b). These contrast $r(\tau)$ and $\phi_1(\tau)$ histories, associated with cases A and B.[1] Note that the $\phi_1$ amplitude of
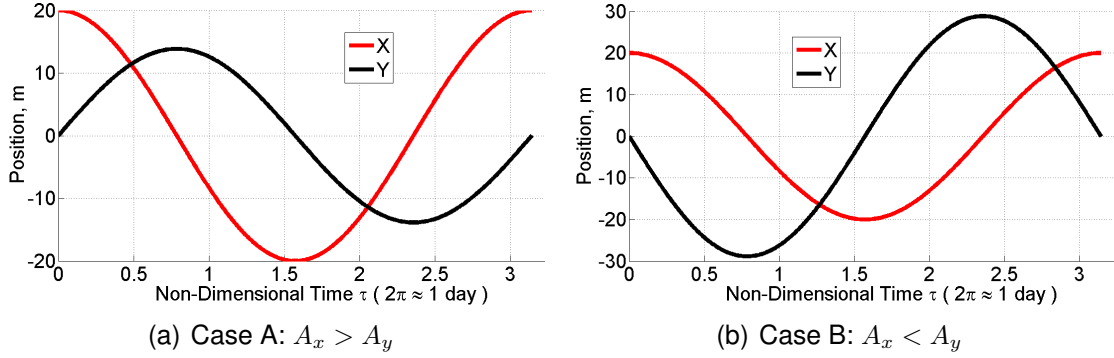


(a) Case A: $A_x > A_y$

(b) Case B: $A_x < A_y$

**Figure 3. Planar Periodic Solution Position Histories:** $A_x = 20$ **m, and** $\tau_p = \pi$



(a) Case A: $A_x > A_y$

(b) Case B: $A_x < A_y$
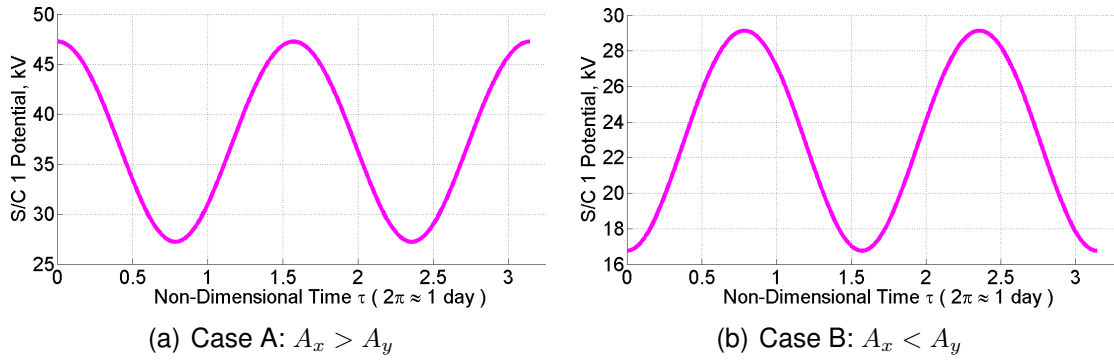
**Figure 4. Planar Periodic Solution Potential Histories:** $A_x = 20$ **m, and** $\tau_p = \pi$

oscillation is greater in case A, despite the case B example representing a larger area ellipse. For either case, the $\phi_1$ amplitude increases in proportion to $A_x$, and inversely with $\tau_p$. Furthermore, the $\phi_1(\tau)$ histories represent very slow $kV$ order transitions (especially since such changes can occur in milliseconds), and are therefore achievable with moderate power (order of Watts).

## 5.2 In-Plane Periodic Motion Stability

Perturbations normal to the orbit plane decouple from the in-plane dynamics (to 1st order), and the two Floquet multipliers associated with orbit-normal perturbations, have modulus of unity. Values of the remaining four multipliers, or Monodramy matrix eigenvalues, are functions of $A_x$, $\tau_p$, and case A/B selection. Numerical trends in the magnitude of $|\sigma|_{\text{max}}$ are summarized as follows.

1. $|\sigma|_{\text{max}} \uparrow$ as $\tau_p \uparrow$ and as $A_x \uparrow$ (weakly for Case A)

2. Case A solutions tend to have much larger $|\sigma|_{\text{max}}$ than case B solutions

---

[1] In Figs. 4(a)-4(b) and subsequent figures, S/C is used as a shorthand for spacecraft.

Additionally, solutions where $\tau_p \ll 2\pi$ yield $|\sigma|_{max} \approx 1$, and therefore quickly oscillating formations are weakly unstable. In Figs. 5(a)-5(b), Monodramy matrix eigenvalues associated with a case B formation are shown in the complex plane, for varying $A_x$ and $\tau_p$. The parameter dependent stability is clear, and it is evident that two of the $\sigma_i$
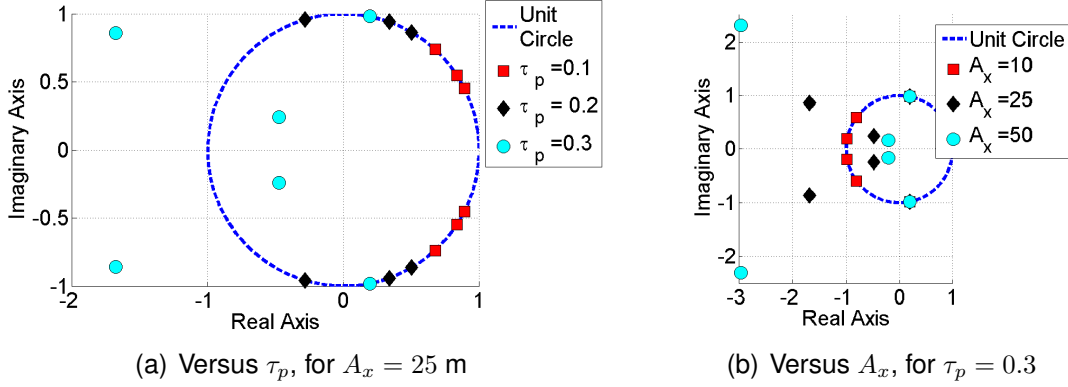


(a) Versus $\tau_p$, for $A_x = 25$ m

(b) Versus $A_x$, for $\tau_p = 0.3$

**Figure 5. Floquet Multipliers in the Complex Plane**

(those associated with $\hat{e}_N$ modes) remain on the unit circle, and move around it with $\tau_p$. It can be inferred from the plots that case B formations, having period less than $1$ hour and separation distance on the order of $10$ meters, exhibit very near marginal stability.

## 5.3  Full State Periodic Motions

An example full state periodic solution is presented in Fig. 6(a)-6(b), for $A_x > A_y$ (case A), $A_x = 20$ m, $A_z = 10$ m, and $B_z = 2$. The required oscillation period (computed numerically) is around $0.73$ days. The craft 1 trajectory for this same example solution
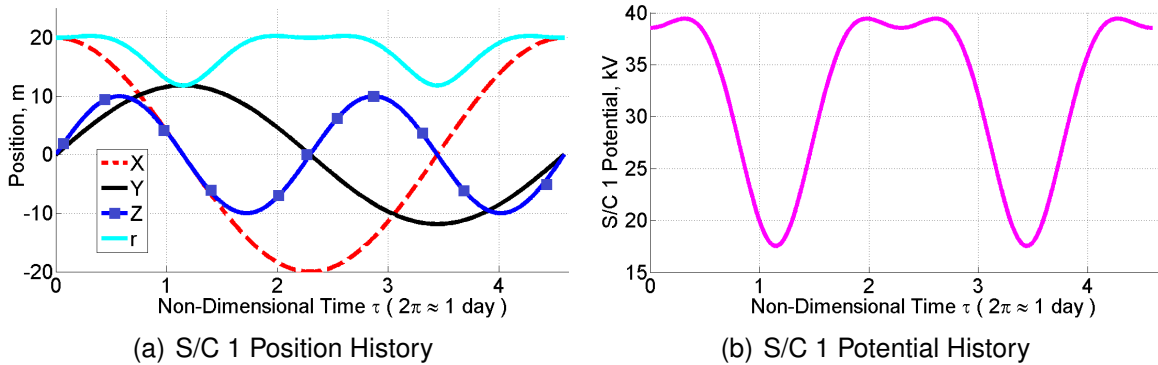


(a) S/C 1 Position History

(b) S/C 1 Potential History

**Figure 6. Full State Periodic Solution:** $A_x = 20$ **m,** $A_z = 10$ **m, and** $B_z = 2$

is shown in Fig. 7(a), and the orbit resembles a saddle shape. A different example trajectory is depicted in Fig. 7(b), which demonstrates some of the rich geometry in these orbit families. This latter example is a case B orbit, generated with the same $A_x$ and $A_z$ (as the case A example), but with $B_z = 4$ and it has a longer period of around $4.4$ days. Some qualitative differences in case B orbits (relative to case A) include a longer $\tau_p$ for the same $|A_x \cdot A_y|$ area, and simple harmonic oscillation for $\phi_1(\tau)$.

14

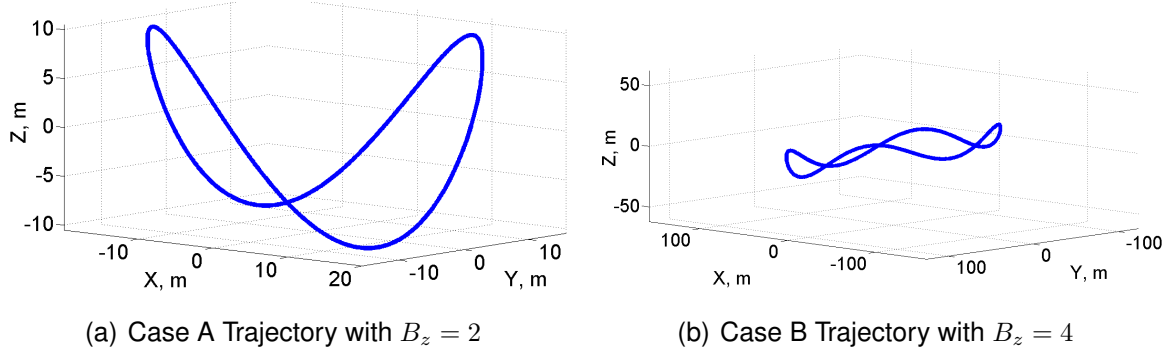(a) Case A Trajectory with $B_z = 2$  (b) Case B Trajectory with $B_z = 4$

**Figure 7. Full State Periodic Solution Trajectories: $A_x = 20$ m and $A_z = 10$ m**

## 5.4 Full State Periodic Motion Stability

For this orbit family, $|\sigma|_{\text{max}}$ is a function of all parameters: $B_z$, $A_x$, $A_z$, and case A/B selection. The following numerical trends (applicable to both case A and B) are identified over varied parameter ranges: $2 \le B_z \le 8$, $10 \le A_x \le 100$ m, and $5 \le A_z \le 80$ m.

1. $|\sigma|_{\text{max}} \uparrow$ as $B_z \uparrow$

2. $|\sigma|_{\text{max}} \uparrow$ as $A_x \uparrow$ (although often weakly)

3. Case A solutions have much larger $|\sigma|_{\text{max}}$ than case B solutions

Again all are Lyapunov unstable, and the most significant parameter driving relative instability is $B_z$. The smallest $|\sigma|_{\text{max}}$ value found for case A orbits is $|\sigma|_{\text{max}} = 3511$, corresponding to $B_z = 2$, $A_x = 50$, and $A_z = 80$. Whereas the case B solutions rendered $1.8 \le |\sigma|_{\text{max}} \le 1500$, with $|\sigma|_{\text{max}} = 1.8$ occurring at $B_z = 2$, $A_x = 10$, and $A_z = 45$.

## 6 Inertial Dynamics with Perturbations

Here an inertial frame dynamical model is developed that includes nonlinear gravity, primary disturbances, and parameter uncertainties. Specifically, absolute solar radiation and an induced perturbation due to uncertainty in the parameter $\lambda_d$ are modeled. The prior Hill frame model trajectories may then be integrated using this higher accuracy model to assess deviations from nominal and to numerically validate qualitative Floquet stability claims.

Referring back to Fig. 2, a spacecraft position vector $\mathbf{R}_i$ with respect to the Earth centered inertial frame $\mathbb{N}$, may be propagated independently in accordance with Eq. (34).

$$\mathbf{R}_i''(\tau) = \frac{\mu}{\omega^2 \, R_i^3} \mathbf{R}_i \; + \frac{\tilde{q}_i}{m_i} \sum_{\substack{j \\ j \ne i}} \frac{\tilde{q}_j \left(1 + \frac{R_{ij}}{\lambda_d}\right) \mathbf{R}_{ij}}{R_{ij}^3 \exp\left[R_{ij}/\lambda_d\right]} + \; \tilde{\mathbf{f}}_{\text{srp}} \tag{34}$$

Where $R_{ij} = \|\mathbf{R}_i - \mathbf{R}_j\|$ is a separation distance (equivalent to $r_{ij}$), $\mu$ is the Earth's gravitational constant, and $\tilde{\mathbf{f}}_{\text{srp}}$ is a scaled solar radiation pressure (SRP) acceleration. Although not explicit, terms on the right hand side are $\tau$ dependent, and the first term is classical gravitational acceleration scaled into non dimensional time. Charge histories $\tilde{q}_i(\tau)$ are known functions assumed to be dependent on a nominal Hill frame model

15

solution $\mathbf{X}^*(\tau)$. Therefore, deviations from $\mathbf{X}^*(\tau)$ due to $\tilde{\mathbf{f}}_{\text{srp}}$, nonlinear gravity terms, and parameter uncertainties are not reflected in the charge control.

The $\mathbf{X}^*(\tau)$ solution contains initial $\mathbf{r}_i$ and $\mathbf{v}_i$, such that initial $\mathbf{R}_i$ are obtained via Eq. (3) (with $\mathbf{R}_{\text{cm}}$ and its derivative specified at the nominal circular reference orbit). Initial $\dot{\mathbf{R}}_i$ are obtained using Eq. (35), again assuming initially aligned $\mathcal{N}$ and $\mathcal{H}$ unit vectors.

$$^{\mathcal{N}}\dot{\mathbf{R}}_i = \dot{\mathbf{R}}_{\text{cm}} + \dot{\mathbf{r}}_i + (\boldsymbol{\omega} \times \mathbf{r}_i) \tag{35}$$

## 6.1 Perturbation Models

The primary disturbing force for Coulomb formations near GEO is SRP[33]. Another very important perturbation modeled and simulated here, is not a physical force but rather the parametric uncertainty in the Debye length. All prior Coulomb formation trajectories assumed a constant nominal $\lambda_d$, but in actuality $\lambda_d$ varies quite significantly in time and space, and therefore it is important to analyze the sensitivity of the solutions to this variation. The cannonball SRP model is naturally adopted for the spherical craft[33], and the unit vector from Sun to Earth is assumed constant over a simulation and in the $\hat{i}$-$\hat{k}$ plane, in accordance with $\mathcal{N}$ being an equatorial frame. A scaled SRP acceleration on craft $i$ is then defined by Eq. (36), where $\Theta = 1372.5398$ W/m$^2$ is the solar flux constant at 1 AU, $c$ is the speed of light, and $C_R$ is the coefficient of reflectivity (an average value based on recent data of $C_R = 1.3$ is assumed).[33, 8]

$$\tilde{\mathbf{f}}_{\text{srp}} = \frac{-1}{\omega^2} \left( \frac{C_R \, \pi R_{sc}^2 \, \Theta}{m_i \, c} \right) \begin{bmatrix} \cos(23.4) \\ 0 \\ \sin(23.4) \end{bmatrix}^{\mathcal{N}} \tag{36}$$

For an $R_{sc} = 1$ m spacecraft this amounts to a force of around 18 $\mu$N.

In Ref. [29], 10-year averaged experimental plasma data are presented, for the GEO regime, versus local time and $K_p$ (an integer index between $0 - 9$, with $1$ being calm and $> 5$ indicating noisy or stormy geomagnetic activity). From these data, Debye length versus $K_p$ is interpolated, at various local times (equivalent to mean anomaly
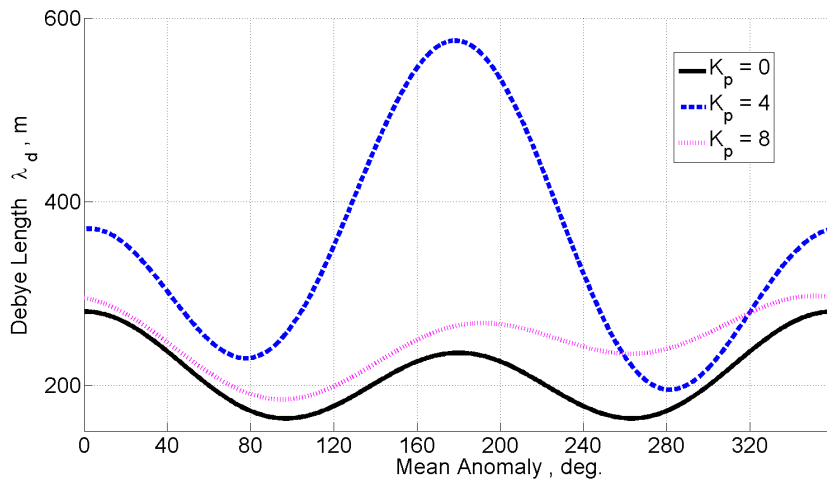


**Figure 8. Interpolated Debye Length at GEO versus Anomaly and $K_p$**

16

for GEO spacecraft). A fast Fourier transform (keeping the first four coefficients) is then applied to that data, for three $K_p$ index values. The resulting analytical interpolated $\lambda_d$ expressions as a function of mean anomaly (equivalent to $\tau$ in radians) are plotted in Fig. 8, where a mean anomaly of $180$ degrees is between the Earth and Sun.

These Fig. 8 interpolated functions are used to simulate realistically possible variations in $\lambda_d$ and the disturbances they generate. Although the true $\lambda_d(\tau)$ can involve stochastic and chaotic behavior, this model does capture the largest magnitude time variations. Therefore, it is deemed sufficient to provide an initial assessment of the sensitivity of open-loop Coulomb formation solutions, to $\lambda_d$ uncertainty.

## 6.2 Transformations from ECI to Hill Frame

Upon integrating via Eq. (34), with some combination of the perturbations developed in Section 6.1, the quantities $\mathbf{R}_i(\tau)$, $\mathbf{R}'_i(\tau)$, $\mathbf{R}_{\text{cm}}(\tau)$, and $\mathbf{R}'_{\text{cm}}(\tau)$ are known (the latter two computed explicitly from former two). To compare these higher fidelity $\mathcal{N}$ frame trajectories to the nominal $\mathcal{H}$ frame trajectories, a transformation must be performed. First, position vectors $^{\mathcal{N}}\mathbf{r}_i(\tau)$ are computed using Eq. (3), and scaled velocity vectors $^{\mathcal{N}}\mathbf{v}_i(\tau)$ are transformed using Eq. (37).

$$^{\mathcal{N}}\mathbf{v}_i = \mathbf{R}'_i - \mathbf{R}'_{\text{cm}} - (\mathbf{n} \times \mathbf{r}_i) \ , \qquad \mathbf{n} = \left( \frac{\mathbf{R}_{\text{cm}} \times \mathbf{R}'_{\text{cm}}}{\|\mathbf{R}_{\text{cm}}\|^2} \right) \tag{37}$$

Where $\mathbf{n}$ is the true angular velocity vector of the $\mathcal{H}$ frame, in contrast to the nominal which is denoted $\boldsymbol{\omega}$. The transformed trajectories are still in the $\mathcal{N}$ frame basis, and therefore the Eq. (38) rotation (transform) matrix $\mathbf{T}$ is applied, such that $^{\mathcal{H}}\mathbf{r}_i = [\mathbf{T}] \ ^{\mathcal{N}}\mathbf{r}_i$ and $^{\mathcal{H}}\mathbf{v}_i = [\mathbf{T}] \ ^{\mathcal{N}}\mathbf{v}_i$.

$$\mathbf{T} = \begin{bmatrix} \hat{\mathbf{T}}_1^T \\ \hat{\mathbf{T}}_2^T \\ \hat{\mathbf{T}}_3^T \end{bmatrix} \qquad \hat{\mathbf{T}}_1 = \frac{\mathbf{R}_{\text{cm}}}{R_{\text{cm}}} \qquad \hat{\mathbf{T}}_2 = \hat{\mathbf{T}}_3 \times \hat{\mathbf{T}}_1 \qquad \hat{\mathbf{T}}_3 = \frac{\mathbf{R}_{\text{cm}} \times \mathbf{R}'_{\text{cm}}}{\|\mathbf{R}_{\text{cm}} \times \mathbf{R}'_{\text{cm}}\|} \tag{38}$$

## 7 Perturbed Coulomb Formation Numerical Simulations

Again all subsequent results are generated using the Table 2 constant values (except of course for varying $\lambda_d$). In order to quantify and compare deviations from nominal, an $L_2$ norm of the absolute error in the craft 1 position vector is computed at the final time $t_f$ (non dimensional $\tau_f$). This measure is denoted $X_{\text{err}}$, and is defined in Eq. (39).

$$X_{\text{err}} = \|\mathbf{r}_1(\tau_f) - \mathbf{r}_1^*(\tau_f)\|_2 \tag{39}$$

Where $\mathbf{r}_1(\tau)$ is a disturbed trajectory position vector (transformed to the Hill frame), and $\mathbf{r}_1^*(\tau)$ is a nominal trajectory position vector obtained within the Section 2 model.

## 7.1 Perturbed In-Plane Periodic Motions

The planar periodic orbits derived in Section 4.1 are first propagated via Eq. (34) with only SRP as a perturbing force (i.e. $\lambda_d$ constant). Some simulation error results are presented in Table 3, which shows case B solutions remain near nominal much longer

**Table 3. In-Plane Periodic Coulomb Formation Deviations with SRP only**

| Case | $A_x$, m | $t_p$, hrs. | $t_f$, hrs. | $X_{\text{err}}$, m |
|------|------|------|------|------|
| A | 20 | 12 | 48 | $1.05e^3$ |
| A | 20 | 2.4 | 48 | $1.11e^2$ |
| A | 50 | 2.4 | 48 | $3.87e^3$ |
| B | 20 | 12 | 48 | $3.65e^{-2}$ |
| B | 20 | 2.4 | 48 | $7.34e^{-3}$ |

than case A solutions. These data validate stability claims made in Section 5.2, including relative instability (measured here by $X_{\text{err}}$) increasing in proportion to $A_x$ and inversely with the relative motion period.

The remaining simulations have variable Debye included (with $K_p = 0$), and some key results are summarized in Table 4. The Debye variation clearly causes greater disturbance (than just SRP), even at relatively quiet $K_p = 0$ geomagnetic conditions. These results also confirm the Section 5.2 relative instability claims, but interestingly the last row in Table 4 shows a solution that deviates no more than tens of centimeters, over a 2 week period.

**Table 4. In-Plane Periodic Coulomb Formation Deviations**

| Case | $A_x$, m | $t_p$, hrs. | $t_f$, hrs. | $X_{\text{err}}$, m |
|------|------|------|------|------|
| A | 20 | 2.4 | 48 | $2.66e^3$ |
| B | 20 | 12 | 48 | $3.33e^2$ |
| B | 20 | 2.4 | 48 | $1.76e^{-1}$ |
| B | 50 | 2.4 | 48 | $2.08e^3$ |
| B | 20 | 2.4 | 336 | $5.75e^{-2}$ |

Relative stability measures laid forth in Section 5.2, are immensely important when considering the feedback control effort required to maintain one of these relative orbit types. To illustrate this point, two perturbed periodic Coulomb formations are shown in Figs. 9-10, with the only difference between them being either case A or case B (i.e. how the major axis is aligned). The case B example corresponds to the last row in Table 4, which exhibited a very small $X_{\text{err}}$. The case A solution wildly departs nominal in less than 10 revolutions (1 day), whereas the case B solution with major axis along $\hat{e}_T$ remains in the vicinity of nominal for 40 revolutions (4 days). This invaluable facet is unique to the periodic Coulomb formations, as all static Coulomb formations (with gravity considered) quickly leave nominal when subjected to a perturbed environment (in fact departing along associated unstable manifolds). Figure 10 provides numerical evidence that a relative Coulomb orbit which has nonlinear open-loop uniform stability may exist (in the Lyapunov sense).[26]
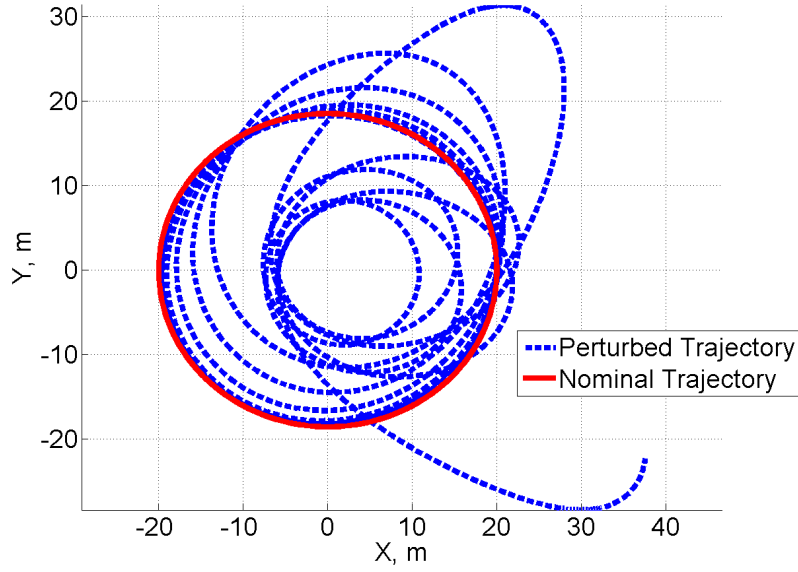
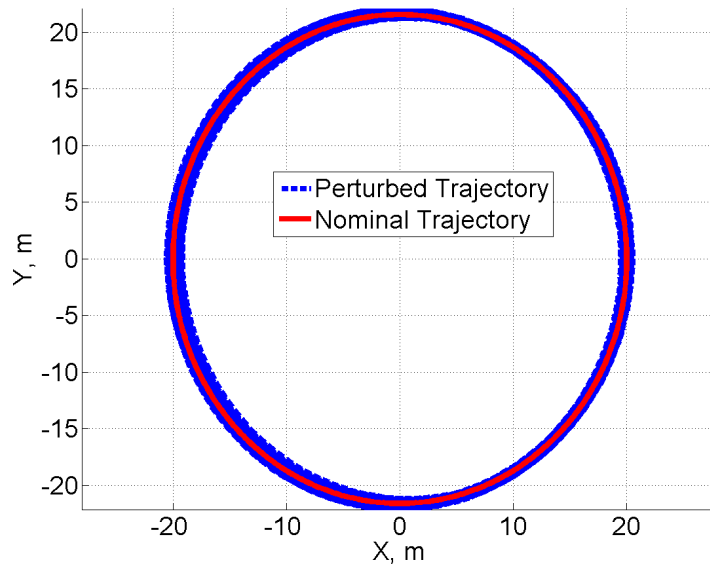**Figure 9. Perturbed Planar Periodic Solution Trajectory for 10 Revolutions: Case A,** $A_x = 20$ **m, and** $t_p = 2.4$ **hrs.**



**Figure 10. Perturbed Planar Periodic Solution Trajectory for 40 Revolutions: Case B,** $A_x = 20$ **m, and** $t_p = 2.4$ **hrs.**

## 7.2   Perturbed Full State Periodic Coulomb Formations

The simulations undertaken in Section 7.1 are continued here, but for the full state solutions derived in Section 4.2. Error results with both SRP and variable Debye length perturbations included are presented in Table 5, and again the induced $\lambda_d(\tau)$ perturbation is found to cause greater deviation than SRP alone. These data very clearly assert that case A solutions, are indeed, relatively more unstable than case B. The additional $|\sigma|_{\text{max}}$ trends identified in Section 5.4 are also reflected here, specifically that $X_{\text{err}}$ increases in proportion to $A_x$ and $B_z$.

**Table 5. Full State Periodic Coulomb Formation Deviations**

| Case | $A_x$, m | $A_z$, m | $B_z$ | $K_p$ | Revs. | $t_f$, hrs. | $X_{\text{err}}$, m |
|------|----------|----------|-------|-------|-------|-------------|---------------------|
| A | 20 | 10 | 2 | 0 | 2.5 | 43.9 | $1.59e^3$ |
| B | 20 | 10 | 2 | 0 | 2 | 98.7 | $3.66e^2$ |
| B | 10 | 45 | 4 | 0 | 1 | 97 | $5.43e^1$ |
| B | 10 | 45 | 2 | 0 | 2 | 98.7 | $4.91e^{-1}$ |
| B | 10 | 45 | 2 | 4 | 2 | 98.7 | $1.85e^1$ |
| B | 10 | 45 | 2 | 8 | 2 | 98.7 | $5.64e^0$ |

For a particular barely unstable solution, the geomagnetic parameter $K_p$ is shown to cause greater deviations during storm conditions, as expected. Much of the focus in Table 5 is devoted to this particular solution, because it corresponds to the smallest $|\sigma|_{\text{max}}$ (least unstable) case found numerically in Section 5.4. This solution is therefore integrated for 6 revolutions (nearly 300 hours), with SRP and Debye variations present ($K_p = 0$), and the resulting perturbed trajectory is plotted alongside nominal in Fig. 11. This is an example of a full state periodic solution that remains in the vicinity of nominal
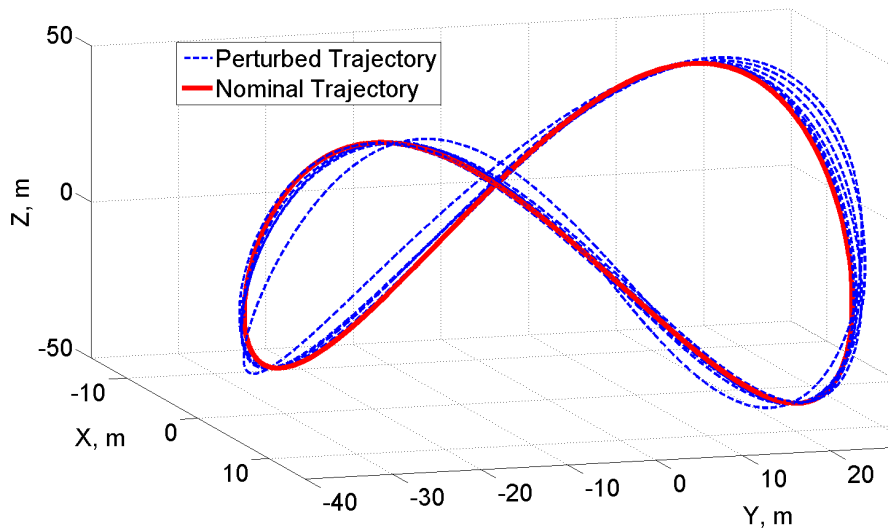


**Figure 11. Perturbed Full State Periodic Solution Trajectory: Case B, $A_x = 10$ m, $A_z = 45$ m, $B_z = 2$, and $t_f = 296.1$ hrs.**

(deviation $< 2.6$ m) for considerable time, without feedback stabilization. Contrast this with the very unstable analogue example shown in Fig. 12, where the case A nominal corresponds to that of Fig. 7(a), from Section 5.3. The Fig. 12 disturbed trajectory exponentially departs in less than half a revolution (less than 18 hours are plotted). Full state periodic solutions tend to have larger $|\sigma|_{\text{max}}$ than do planar solutions, and this greater instability is generally brought out in numerical simulation. However, interestingly there do exist full state periodic solutions, as in Fig. 11, which remain in the vicinity of nominal for long duration, when subjected to primary perturbations.
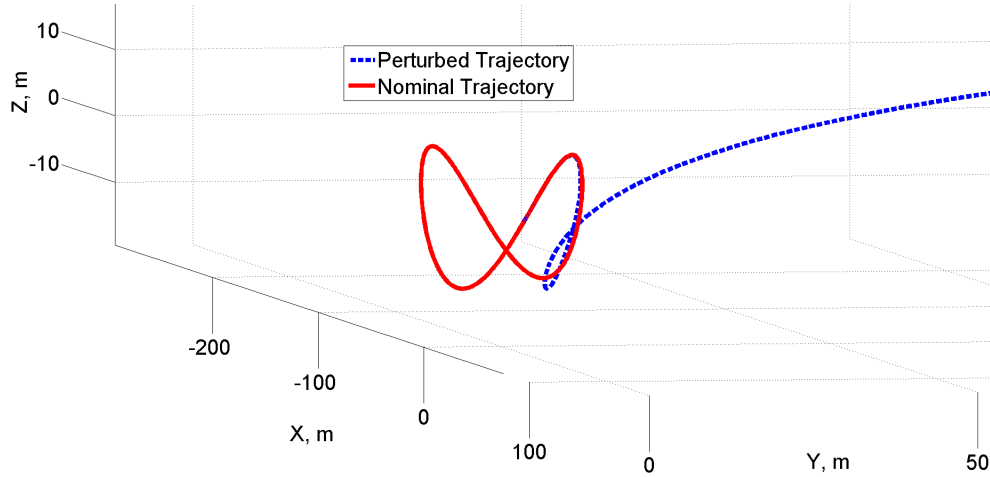
**Figure 12. Perturbed Full State Periodic Solution Trajectory: Case A,** $A_x = 20$ **m,** $A_z = 10$ **m,** $B_z = 2$**, and** $t_f = 17.6$ **hrs.**

## 8  Conclusions

The existence of dynamic and periodic Coulomb formations are demonstrated for two spacecraft in the Hill frame with differential gravity. These are the first demonstrated examples of repeating relative orbit motions, in which the charge is dynamically varied in open-loop to produce the forcing. The required variations are slow kV order transitions, and are therefore readily achievable with moderate power (order of Watts). The results provide a valuable extension to the many works concerning static Coulomb formations (fixed distances and constant potentials).

Some possible applications for these near propellantless relative orbits include interferometry with variable separation distance (and optionally an inertially fixed line-of-sight vector), Earth/Sun imaging, and autonomous inspection of a cooperating or non cooperating vehicle. Detailed examinations into utilizing these electrostatic forced periodic solutions, should be considered in future research. The open-loop orbits would, of course, require feedback stabilization. Hence, the varied relative instability demonstrated here would be crucial in selecting particular solutions, and in the development of station-keeping control.

This investigation restricts attention to 2-craft formations with approximate dynamics, and so future research should attempt to derive analogous oscillatory flows for 3-craft (or even N-craft) Coulomb formations, within this dynamical model or otherwise (e.g. higher order gravity or CRTBP). However, periodic craft trajectories are non arbitrary, and the full set of solutions will exist as a subset of some finite Fourier series representation. Future research should determine the existence of these hypothesized solutions, and the Hill frame integral of motion should help facilitate such efforts. Quasi-periodic solutions should also be considered, and these could include numerically targeted solutions or simply those orbits which result from integrating exact periodic solutions using higher order perturbed dynamics.

The accuracy of these periodic solutions are analyzed, by considering solar radiation pressure and using an interpolated variable Debye length model, developed here. Of

course, feedback stabilization could still overcome such disturbances; however, in general this would require some inertial thrusting. Therefore, all the more important are those periodic Coulomb formations shown to remain in the vicinity of nominal, for many relative orbit cycles, in a higher fidelity environment. The results suggest improved stability (certain cases) in these periodic relative motion solutions, compared with static equilibria solutions. Moreover, particular solutions seem to exhibit uniform stability in the perturbed nonlinear environment, and therefore may have advantageous application. For example, to provide a low cost means of allowing multiple spacecraft to share a single Geostationary slot. However, the adopted model does not reflect all perturbations nor other higher order aspects of the electrostatic model. Such considerations, although interesting, are beyond the scope intended here, but should be pondered for extended research.

## Acknowledgments

## References

[1] Cover, J. H., Knauer, W., and Maurer, H. A., "Lightweight Reflecting Structures Utilizing Electrostatic Inflation," US Patent 3,546,706, October 1966.

[2] King, L., Parker, C., Deshmukh, S., and Chong, J., "Spacecraft Formation-flying Using Inter-vehicle Coulomb Forces," Tech. rep., NASA Institute for Advanced Concepts, January 2002.

[3] King, L., Parker, C., Deshmukh, S., and Chong, J., "Study of Interspacecraft Coulomb Forces and Implications for Formation Flying," *Journal of Propulsion and Power*, Vol. 19, No. 3, 2003, pp. 497–505, doi: 10.2514/2.6133.

[4] Schaub, H., Parker, G., and King, L., "Challenges and Prospects of Coulomb Spacecraft Formation Control," *Journal of the Astronautical Sciences*, Vol. 52, No. 1-2, 2004, pp. 169–193.

[5] Mullen, E., Gussenhoven, M., and Hardy, D., "SCATHA," *Journal of the Geophysical Sciences*, Vol. 91, No. A2, 1986, pp. 1474–1490.

[6] Whipple, E. and Olsen, R., "Importance of Differential Charging for Controlling Both Natural and Induced Vehicle Potentials on ATS-5 and ATS-6," *Proceedings of the 3rd Spacecraft Charging Technology Conference*, 1980, pp. 888–893.

[7] Escoubet, C., Fehringer, M., and Goldstein, M., "The Cluster Mission," *Annales Geophysicae*, Vol. 19, No. 10/12, 2001, pp. 1197–1200.

[8] Moorer, D. and Schaub, H., "Geosynchronous Large Debris Reorbiter: Challenges and Prospects," *AAS/AIAA Kyle T. Alfriend Astrodynamics Symposium*, No. 10-311, May 2010, Monterey, CA.

[9] Berryman, J. and Schaub, H., "Analytical Charge Analysis for Two- and Three-Craft Coulomb Formations," *Journal of Guidance, Control, and Dynamics*, Vol. 30, No. 6, 2007, pp. 1701–1710, doi: 10.2514/1.23785.

[10] Schaub, H. and Kim, M., "Differential Orbit Element Constraints for Coulomb Satellite Formations," *AIAA/AAS Astrodynamics Specialists Conference*, No. 04-5213, August 2004, doi: 10.2514/6.2004-5213.

[11] Stiles, L., Seubert, C., and Schaub, H., "Effective Coulomb Force Modeling in a Space Environment," *AAS/AIAA Spaceflight Mechanics Meeeting*, No. 12-105, January-February 2012, Charleston, SC.

[12] Seubert, C., Panosian, S., and Schaub, H., "Attitude and Power Analysis of Two-Node, Multi-Tethered Coulomb Structures," *Journal of Spacecraft and Rockets*, Vol. 48, No. 6, 2011, pp. 1033–1045, doi: 10.2514/1.52185.

[13] Pettazzi, L., Kruger, H., Theil, S., and Izzo, D., "Electrostatic Forces for Satellite Swarm Navigation and Reconfiguration," Tech. Rep. ARIADNA 05/4107a., European Space Agency, 2006.

[14] Bittencourt, J., *Fundamentals of Plasma Physics*, Springer-Verlag New York, Inc., 2004.

[15] Natarajan, A., *A Study of Dynamics and Stability of Two-Craft Coulomb Tether Formations*, Ph.D. thesis, Virginia Polytechnic Institute and State University, 2007.

[16] Jones, D. R. and Schaub, H., "Collinear Three-Craft Coulomb Formation Stability Analysis and Control," *AIAA/AAS Astrodynamics Specialists Conference*, No. 12-4721, August 2012, Minneapolis, MN, doi: 10.2514/6.2012-4741.

[17] Hussein, I. I. and Schaub, H., "Stability and Control of Relative Equilibria for the Three-Spacecraft Coulomb Tether Problem," *Acta Astronautica*, Vol. 65, No. 5–6, 2009, pp. 738–754, doi: 10.1016/j.actaastro.2009.03.035.

[18] Wang, S. and Schaub, H., "Nonlinear Charge Control for a Collinear Fixed-Shape Three-Craft Equilibrium," *Journal of Guidance, Control, and Dynamics*, Vol. 34, No. 2, 2011, pp. 356–366, doi: 10.2514/1.52117.

[19] Schaub, H. and Hussein, I. I., "Stability and Reconfiguration Analysis of a Circulary Spinning Two-Craft Coulomb Tether," *IEEE Transactions on Aerospace and Electronic Systems*, Vol. 46, No. 4, 2010, pp. 1675–1686.

[20] Hogan, E. and Schaub, H., "Linear Stability and Shape Analysis of Spinning Three-Craft Coulomb Formations," *Celestial Mechanics and Dynamical Astronomy*, Vol. 112, No. 2, 2012, pp. 131–148, doi: 10.1007/s10569-011-9387-6.

[21] Berryman, J. and Schaub, H., "Static Equilibrium Configurations in GEO Coulomb Spacecraft Formations," *AAS/AIAA Space Flight Mechanics Meeting*, No. 05-104, January 2005, Copper Mountain, CO.

[22] Jones, D. R. and Schaub, H., "Periodic Relative Orbits of Two Spacecraft Subject to Differential Gravity and Electrostatic Forcing," *Acta Astronautica*, 2013, pp. 21–30, doi: 10.1016/j.actaastro.2013.03.028.

[23] Jasch, P., Hogan, E., and Schaub, H., "Stability Analysis and Out-of-Plane Control of Collinear Spinning Three-Craft Coulomb Formations," *AAS/AIAA Spaceflight Mechanics Meeting*, No. 12-151, January-February 2012, Charleston, SC.

[24] Lee, D.-H., Kumar, K., and Bang, H., "Formation Flying of Small Satellites Using Coulomb Forces," *International Journal of Aeronautical and Space Science*, Vol. 7, No. 1, 2006, pp. 84–90, doi : 10.5139/IJASS.2006.7.1.084.

[25] Floquet, G., "Sur les quations diffrentielles linaires  coefficients priodiques," *Annales de l'cole Normale Suprieure*, Vol. 12, 1883, pp. 47–88.

[26] Meirovitch, L., *Methods of Analytical Dynamics*, McGraw-Hill, 1970, pp. 264–276.

[27] Szebehely, V., *Theory of Orbits: The Restricted Problem of Three Bodies*, Academic Press, New York, 1967.

[28] Saaj, C., Lappas, V., Richie, D., Peck, M., Streetman, B., and Schaub, H., "Electrostatic Forces for Satellite Swarm Navigation and Reconfiguration," Tech. Rep. ARIADNA 05/4107b., European Space Agency, 2006.

[29] Denton, M., Thomsen, M., Korth, H., Lynch, S., Zhang, J., and Liemohn, M., "Bulk Plasma Properties at Geosynchronous Orbit," *Journal of Geophysical Research*, Vol. 110, No. A07223, 2005, doi: 10.1029/2004JA010861.

[30] Peck, M., "Prospects and Challenges for Lorentz-Augmented Orbits," *AIAA Guidance, Navigation, and Control Conference*, August 2005, San Francisco, CA, doi: 10.2514/6.2005-5995.

[31] Stevenson, D. and Schaub, H., "Multi-Sphere Method for Modeling Electrostatic Forces and Torques," *Journal of Advances in Space Research*, Vol. 51, No. 1, 2013, pp. 10–20.

[32] Duffin, W., *Electricity and Magnetism*, John Wiley and Sons, New York, NY, 2nd ed., 1973, pp. 83–85.

[33] Romanelli, C., Natarajan, A., Schaub, H., Parker, G., and King, L., "Coulomb Spacecraft Voltage Study Due to Differential Orbital Perturbation," *AAS/AIAA Space Flight Mechanics Meeting*, January 2006, Tampa, FL.

[34] Clohessy, W. and Wiltshire, R., "Terminal Guidance System for Satellite Rendevous," *Journal of the Aerospace Sciences*, Vol. 27, No. 9, 1960, pp. 653–658, doi: 10.2514/8.8704.

[35] Norman, M. and Peck, M., "Integrals of Motion for Planar Multi-Body Formations with Internal Forces," *Journal of Guidance, Control, and Dynamics*, Vol. 34, No. 6, 2011, pp. 1790–1797.

[36] Vadali, S., Schaub, H., and Alfriend, K., "Initial Conditions and Fuel-Optimal Control for Formation Flying of Satellites," *AIAA Guidance, Navigation, and Control Conference*, August 1999, Portland, OR.

[37] Perko, L., *Differential Equations and Dynamical Systems*, Springer, 1996, pp. 199–206.